# Effect of Doppler broadening on giant self-Kerr nonlinearity in a five-level ladder-type system

**Nguyen Huy Bang,**[1] **Dinh Xuan Khoa,**[1] **Doan Hoai Son,**[2] **and Le Van Doai**[1,*]

[1]*Department of Physics, Vinh University, 182 Le Duan Street, Vinh City, Vietnam*
[2]*Ha Tinh Universiy, Cam Xuyen District, Ha Tinh Province, Vietnam*
*Corresponding author: doailv@vinhuni.edu.vn*

In this paper, we propose an analytical model to study the effect of Doppler broadening on self-Kerr nonlinearity in a five-level ladder-type atomic system. First- and third-order susceptibilities and the self-Kerr nonlinear coefficient are found as the function of temperature and parameters of laser fields. The analytical model is applied to hot $^{85}$Rb and $^{87}$Rb atoms, and it is shown that under the electromagnetically induced transparency (EIT) effect, the self-Kerr nonlinear coefficient is enhanced around three transparent spectral regions. When the temperature of atomic vapor increases (i.e., Doppler width increases), the depth and width of the EIT windows decrease accordingly, and therefore the amplitude of the Kerr nonlinear coefficient decreases significantly. In addition, because the frequency gaps between hyperfine levels of upper excited state $5D_{5/2}$ of $^{85}$Rb atoms are much smaller than those of $^{87}$Rb atoms, the EIT windows as well as the nonlinear dispersion curves for $^{85}$Rb atoms are closer than those for $^{87}$Rb atoms as the Doppler effect presents. The analytical results agree well with the experimental observation when reducing to a three-level atomic system. The analytical model can be used to easily fit the experimental observations of self-Kerr nonlinearity in a five-level atomic system under different temperature conditions and apply to a variety of applications relating to all-optical-switching techniques. © 2019 Optical Society of America

## 1. INTRODUCTION

It is well known that third-order Kerr nonlinearity plays an important role in nonlinear optics [1]. In the past few decades, the discovery of the electromagnetically induced transparency (EIT) [2] effect has led to the large enhancement of the Kerr nonlinear coefficient with low light intensity and reducing absorption [3]. In particular, giant cross-Kerr nonlinearity in EIT medium was first suggested by Schmidt and Imamoglu [4] and has been experimentally measured by Kang and Zhu [5], whereas Wang *et al.* first directly measured the large self-Kerr nonlinear coefficient by using an optical ring cavity [6]. Such an enhanced Kerr nonlinearity can increase conversion efficiency of the nonlinear optical processes at low light levels, such as controlled-NOT (CNOT) gates [7], quantum phase gates [8], frequency conversion [9], optical solitons [10], all-optical switching [11], optical bistability [12,13], and so on.

Early research work on the EIT and the enhancement of self-Kerr nonlinearity has been done for three-level atomic systems, including Λ-, ladder-, and V-type configurations [14–17]. This work shows that the Kerr nonlinearity is only enhanced around a transparent spectral region, that is, the occurrence of a positive–negative pair of nonlinear coefficients around the EIT window. However, recent studies on the EIT

[18–22] and self-Kerr nonlinearity [23–28] have been focused on multi-level atomic systems (four-level, five-level, and six-level systems) to generate multiple EIT windows, and therefore the Kerr nonlinearity is also enhanced at multiple frequency regions. In general, there are two ways to create multiple EIT windows. The first is to use many coupling laser fields to excite many atomic transitions; for example, McGloin *et al.* [18] theoretically studied an $N$-level atomic system excited by $N-1$ coupling laser fields and found $(N-2)$ EIT windows. The second way is to use only a coupling laser field to excite closely spaced hyperfine atomic levels; for example, Wang *et al.* [20] experimentally studied the EIT in a multi-level cascade system of cold $^{85}$Rb atoms and obtained three EIT windows, and Khoa *et al.* [22] measured three-window EIT spectrum in hot $^{85}$Rb atomic vapors.

So far, there have been some theoretical studies on the enhancement of Kerr nonlinearity in multi-level atomic systems using several coupling laser fields [23–27], and a one coupling laser field [28] is proposed. However, most of these works have often neglected the effect of Doppler broadening and therefore the obtained results are only suitable for cold atoms confined in a magneto-optical trap (MOT). There are also some experimental studies of Kerr nonlinear coefficients carried out for hot

atoms [6,17,26,27], and experimental results were simulated by numerical method with good agreement. However, there is still a lack of analytical representation of the Kerr nonlinear coefficient in the presence of Doppler broadening. Such an analytical model not only provides a precise understanding of the Kerr nonlinear coefficient as a function of laser fields and the temperature of medium but is also easily used to fit the experimental results and study applications relating to all-optical-switching techniques [29].

In this work, we develop an analytical model to study the influence of Doppler broadening on self-Kerr nonlinearity of a five-level ladder-type atomic system using one coupling laser field. First- and third-order susceptibilities and the self-Kerr nonlinear coefficient are found as the function of temperature and parameters of laser fields. Influences of temperature and laser parameters on the Kerr nonlinear coefficient of $^{85}$Rb and $^{87}$Rb atoms are studied. The calculated results are also compared with experimental results when reducing to the three-level system.

## 2. THEORETICAL MODEL

The interaction of two laser fields with a five-level ladder-type atomic system composed of a ground state $|1\rangle$, an intermediate state $|2\rangle$, and three excited states $|3\rangle$, $|4\rangle$ and $|5\rangle$ is shown in Fig. 1. Here, three states $|3\rangle$, $|4\rangle$ and $|5\rangle$ are closely spaced hyperfine levels that have the frequency gaps between the levels $|3\rangle - |4\rangle$ and $|5\rangle - |3\rangle$ as $\delta_1$ and $\delta_2$, respectively. A weak probe field with Rabi frequency $\Omega_p$ interacts with the $|1\rangle \rightarrow |2\rangle$ transition, while an intense coupling laser field with Rabi frequency $\Omega_c$ couples the transitions $|2\rangle \rightarrow |3\rangle$, $|2\rangle \rightarrow |4\rangle$, and $|2\rangle \rightarrow |5\rangle$ simultaneously.

In rotating wave approximation, the evolution of the system is given by the full set of density matrix equations as follows [28]:
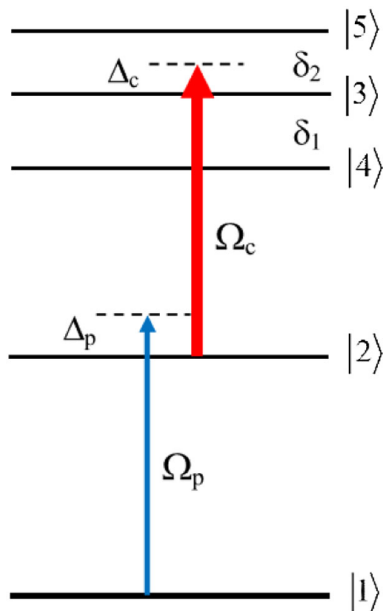


**Fig. 1.** Five-level ladder-type atomic system driven by two laser fields.

$$\dot{\rho}_{55} = -\Gamma_{52}\rho_{55} + \frac{i}{2}\Omega_c a_{52}(\rho_{52} - \rho_{25}), \tag{1}$$

$$\dot{\rho}_{44} = -\Gamma_{42}\rho_{44} + \frac{i}{2}\Omega_c a_{42}(\rho_{42} - \rho_{24}), \tag{2}$$

$$\dot{\rho}_{33} = -\Gamma_{32}\rho_{33} + \frac{i}{2}\Omega_c a_{32}(\rho_{32} - \rho_{23}), \tag{3}$$

$$\dot{\rho}_{22} = -\Gamma_{21}\rho_{22} + \Gamma_{32}\rho_{33} + \Gamma_{42}\rho_{42} + \Gamma_{52}\rho_{52}$$
$$+ \frac{i}{2}\Omega_p(\rho_{21} - \rho_{12}) + \frac{i}{2}\Omega_c a_{32}(\rho_{32} - \rho_{23})$$
$$+ \frac{i}{2}\Omega_c a_{42}(\rho_{42} - \rho_{24}) + \frac{i}{2}\Omega_c a_{52}(\rho_{52} - \rho_{25}), \tag{4}$$

$$\dot{\rho}_{11} = \Gamma_{21}\rho_{22} + \frac{i}{2}\Omega_p(\rho_{12} - \rho_{21}), \tag{5}$$

$$\dot{\rho}_{54} = [-i(\delta_1 + \delta_2) - \gamma_{43}]\rho_{54} + \frac{i}{2}\Omega_c a_{42}\rho_{52}$$
$$- \frac{i}{2}\Omega_c a_{52}\rho_{24}, \tag{6}$$

$$\dot{\rho}_{53} = [-i\delta_2 - \gamma_{53}]\rho_{53} + \frac{i}{2}\Omega_c a_{32}\rho_{52} - \frac{i}{2}\Omega_c a_{52}\rho_{23}, \tag{7}$$

$$\dot{\rho}_{52} = [i(\Delta_c - \delta_2) - \gamma_{52}]\rho_{52} + \frac{i}{2}\Omega_p\rho_{51} + \frac{i}{2}\Omega_c a_{32}\rho_{53}$$
$$+ \frac{i}{2}\Omega_c a_{42}\rho_{54} + \frac{i}{2}\Omega_c a_{52}(\rho_{55} - \rho_{22}), \tag{8}$$

$$\dot{\rho}_{51} = [i(\Delta_p + \Delta_c - \delta_2) - \gamma_{51}]\rho_{51} + \frac{i}{2}\Omega_p\rho_{52}$$
$$- \frac{i}{2}\Omega_c a_{52}\rho_{21}, \tag{9}$$

$$\dot{\rho}_{42} = [i(\Delta_c + \delta_1) - \gamma_{42}]\rho_{42} + \frac{i}{2}\Omega_p\rho_{41} + \frac{i}{2}\Omega_c a_{32}\rho_{43}$$
$$+ \frac{i}{2}\Omega_c a_{52}\rho_{45} + \frac{i}{2}\Omega_c a_{42}(\rho_{44} - \rho_{22}), \tag{10}$$

$$\dot{\rho}_{41} = [i(\Delta_p + \Delta_c + \delta_1) - \gamma_{41}]\rho_{41} + \frac{i}{2}\Omega_p\rho_{42}$$
$$- \frac{i}{2}\Omega_c a_{42}\rho_{21}, \tag{11}$$

$$\dot{\rho}_{34} = [-i\delta_2 - \gamma_{34}]\rho_{34} + \frac{i}{2}\Omega_c a_{42}\rho_{32} - \frac{i}{2}\Omega_c a_{32}\rho_{24}, \tag{12}$$

$$\dot{\rho}_{32} = [i\Delta_c - \gamma_{32}]\rho_{32} + \frac{i}{2}\Omega_p\rho_{31} + \frac{i}{2}\Omega_c a_{32}(\rho_{33} - \rho_{22})$$
$$+ \frac{i}{2}\Omega_c a_{42}\rho_{34} + \frac{i}{2}\Omega_c a_{52}\rho_{35}, \tag{13}$$

$$\dot{\rho}_{31} = [i(\Delta_p + \Delta_c) - \gamma_{31}]\rho_{31} + \frac{i}{2}\Omega_p\rho_{32} - \frac{i}{2}\Omega_c a_{32}\rho_{21} \tag{14}$$

$$\dot{\rho}_{21} = [i\Delta_p - \gamma_{21}]\rho_{21} + \frac{i}{2}\Omega_p(\rho_{22} - \rho_{11}) - \frac{i}{2}a_{32}\Omega_c\rho_{31}$$

$$- \frac{i}{2}\Omega_c a_{42}\rho_{41} - \frac{i}{2}\Omega_c a_{52}\rho_{51}. \tag{15}$$

The above equations are constrained by $\sum_{n=1}^{5}\rho_{nn} = 1$ and $\rho_{mn} = \rho_{nm}^{*}$. Here, $\Delta_p = \omega_p - \omega_{21}$ and $\Delta_c = \omega_c - \omega_{32}$ are the detuning of the probe and the coupling fields, respectively. The Rabi frequencies are given by $\Omega_p = d_{21}E_p/\hbar$ and $\Omega_c = d_{32}E_c/\hbar$ with $d_{21}$ and $d_{32}$ denoting the electric dipole matrix elements. The strengths of the atom-field coupling between the transitions $|2\rangle \leftrightarrow |3\rangle$, $|2\rangle \leftrightarrow |4\rangle$, and $|2\rangle \leftrightarrow |5\rangle$ are characterized by the ratio of electric dipole moments $a_{32} = d_{32}/d_{32}$, $a_{42} = d_{42}/d_{32}$, and $a_{52} = d_{52}/d_{32}$. $\Gamma_{mn}$ denotes the population decay rate of the excited state, whereas $\gamma_{mn} = \Gamma_{mn}/2$ is the coherence atomic decay rate.

To derive the linear and nonlinear susceptibilities, we need to find the steady-state solution of the density-matrix equations up to high-order perturbations. From the above density matrix equations, we found the solution for the density matrix element $\rho_{21}$ (which corresponds to the probe response) in the first- and third-order perturbations as [28]

$$\rho_{21}^{(1)} = \frac{i\Omega_p(\rho_{22}^{(0)} - \rho_{11}^{(0)})}{2F}, \tag{16}$$

$$\rho_{21}^{(3)} = -\frac{i\Omega_p}{2F}\frac{\Omega_p^2}{2\Gamma_{21}}\left(\frac{1}{F} + \frac{1}{F^*}\right), \tag{17}$$

where

$$F = \gamma_{21} - i\Delta_p + \frac{a_{32}^2(\Omega_c/2)^2}{\gamma_{31} - i(\Delta_p + \Delta_c)}$$

$$+ \frac{a_{42}^2(\Omega_c/2)^2}{\gamma_{41} - i(\Delta_p + \Delta_c + \delta_1)} + \frac{a_{52}^2(\Omega_c/2)^2}{\gamma_{51} - i(\Delta_p + \Delta_c - \delta_2)} \tag{18}$$

and $F^*$ is the complex conjugation of $F$.

The solution of the density matrix element $\rho_{21}$ is therefore calculated up to third order as

$$\rho_{21} = \rho_{21}^{(1)} + \rho_{21}^{(3)} = \frac{i\Omega_p}{2F} - \frac{i\Omega_p}{2F}\left[\frac{\Omega_p^2}{2\Gamma_{21}}\left(\frac{1}{F} + \frac{1}{F^*}\right)\right]. \tag{19}$$

Thus, the susceptibility of the atomic medium is related to the density matrix element $\rho_{21}$ by the following relationship:

$$\chi = -2\frac{Nd_{21}}{\varepsilon_0 E_p}\rho_{21} \equiv \frac{i Nd_{21}^2}{\varepsilon_0\hbar F}$$

$$- \left[\frac{i Nd_{21}^4}{\varepsilon_0\hbar^3}\frac{1}{2\Gamma_{21}}\frac{1}{F}\left(\frac{1}{F} + \frac{1}{F^*}\right)\right]E_p^2. \tag{20}$$

However, for centersymmetry medium, the total susceptibility can be extracted into linear and nonlinear terms as follows:

$$\chi = \chi^{(1)} + 3E_p^2\chi^{(3)}. \tag{21}$$

Therefore, the first- and third-order susceptibilities $\chi^{(1)}$ and $\chi^{(3)}$ can be obtained according to the following expressions:

$$\chi^{(1)} = \frac{i Nd_{21}^2}{\varepsilon_0\hbar}\frac{1}{F}, \tag{22}$$

$$\chi^{(3)} = -\frac{i Nd_{21}^4}{3\varepsilon_0\hbar^3}\frac{1}{2\Gamma_{21}}\frac{1}{F}\left(\frac{1}{F} + \frac{1}{F^*}\right). \tag{23}$$

In the above derivations, we ignored the Doppler broadening. For hot atoms, therefore, it is necessary to take into account Doppler broadening. To eliminate the first-order Doppler effect in our experimental scheme, we consider the coupling field is counter-propagating with the probe field in the medium, and their frequencies are very close. Therefore, an atom with velocity $v$ moving toward the probe beam will see the up-shift frequency of the probe beam as $\omega_p + (v/c)\omega_p$ and see the down-shift frequency of the coupling beam as $\omega_c - (v/c)\omega_c$. In such a case, the frequency detuning of the laser beams is adjusted accordingly as $\Delta'_p = \Delta_p + (v/c)\omega_p$ and $\Delta'_c = \Delta_c - (v/c)\omega_c$. The numbers of atoms having velocity $v$ that lie along the beams obey a Maxwellian distribution:

$$dN(v) = \frac{N_0}{u\sqrt{\pi}}e^{-v^2/u^2}dv, \tag{24}$$

where $u = \sqrt{3k_B T/m}$ is the root mean square atomic velocity, and $N_0$ is the total atomic density of the atomic medium. For an inhomogeneously broadened medium, the full width at half-maximum of the absorption line can be given by

$$W_D = \frac{2\omega_p}{c}u\sqrt{\ln 2}. \tag{25}$$

Thus, the susceptibility expressions must be modified to

$$\chi^{(1)}(v)dv = \frac{i N_0 d_{21}^2}{u\sqrt{\pi}\varepsilon_0\hbar}\frac{e^{-v^2/u^2}}{F(v)}dv, \tag{26}$$

$$\chi^{(3)}(v)dv = -\frac{i N_0 d_{21}^4}{3u\sqrt{\pi}\varepsilon_0\hbar^3}\frac{1}{2\Gamma_{21}}\frac{e^{-v^2/u^2}}{F(v)}$$

$$\times \left[\frac{1}{F(v)} + \frac{1}{F^*(v)}\right]dv, \tag{27}$$

where

$$F(v) = \gamma_{21} - i\left(\Delta_p + \frac{v}{c}\omega_p\right)$$

$$+ \frac{a_{32}^2(\Omega_c/2)^2}{\gamma_{31} - i(\Delta_p + \Delta_c) - i\frac{v}{c}(\omega_p - \omega_c)}$$

$$+ \frac{a_{42}^2(\Omega_c/2)^2}{\gamma_{41} - i(\Delta_p + \Delta_c + \delta_1) - i\frac{v}{c}(\omega_p - \omega_c)}$$

$$+ \frac{a_{52}^2(\Omega_c/2)^2}{\gamma_{51} - i(\Delta_p + \Delta_c - \delta_2) - i\frac{v}{c}(\omega_p - \omega_c)}. \tag{28}$$

Because $\omega_p$ is very close to $\omega_c$, the expressions (26) and (27) become

$$\chi^{(1)}(x)dx = \frac{iN_0 d_{21}^2}{\sqrt{\pi}\varepsilon_0\hbar\left(\omega_p u/c\right)}\frac{e^{-x^2}}{(z-ix)}dx, \quad (29)$$

$$\chi^{(3)}(x)dx = -\frac{iN_0 d_{21}^4}{3\sqrt{\pi}\varepsilon_0\hbar^3\left(\omega_p u/c\right)^2}\frac{1}{2\Gamma_{21}}\frac{e^{-x^2}}{(z-ix)}$$

$$\times\left[\frac{1}{(z-ix)}+\frac{1}{(z^*+ix)}\right]dx, \quad (30)$$

where $x = v/u$ and

$$z = \frac{c}{\omega_p u}F. \quad (31)$$

$F$ is determined from expression (18), and $z^*$ is the complex conjugation of $z$.

By integrating the expressions (29) and (30) over the velocity $v$ from $-\infty$ to $+\infty$, we obtain the expressions for first- and third-order susceptibilities under Doppler broadening as

$$\chi^{(1)} = \frac{iN_0 d_{21}^2\sqrt{\pi}}{\varepsilon_0\hbar\left(\omega_p u/c\right)}e^{z^2}[1-\text{erf}(z)], \quad (32)$$

$$\chi^{(3)} = -\frac{iN_0 d_{21}^4}{3\sqrt{\pi}\varepsilon_0\hbar^3\left(\omega_p u/c\right)^2}\frac{1}{2\Gamma_{21}}$$

$$\left\{2\sqrt{\pi}\left(-1+\sqrt{\pi}ze^{z^2}[1-\text{erf}(z)]\right)\right.$$

$$\left.+\frac{\pi\left(e^{z^2}[1-\text{erf}(z)]+e^{z^{*2}}[1-erf(z^*)]\right)}{z+z^*}\right\}, \quad (33)$$

where erf(z) is the error function, which is determined by

$$\text{erf}(z) = \frac{2}{\sqrt{\pi}}\int_0^z e^{-t^2}dt. \quad (34)$$

From the first- and third-order susceptibilities, we find the absorption $(\alpha)$, dispersion $(n_0)$, and self-Kerr nonlinear $(n_2)$ coefficients under Doppler broadening as [1]

$$\alpha = \frac{\omega_p\,\text{Im}(\chi^{(1)})}{c}, \quad (35)$$

$$n_0 = 1+\frac{1}{2}\text{Re}(\chi^{(1)}), \quad (36)$$

$$n_2 = \frac{3\,\text{Re}(\chi^{(3)})}{4\varepsilon_0 n_0^2 c}. \quad (37)$$

From the obtained results we note that, first, although this configuration uses only one coupling laser beam, and it can therefore be applied to the case of closely spaced hyperfine atomic levels, if the excited states are far apart, the model can still be used by assuming the coupling laser beam corresponding to three independent lasers $\Omega_1 = a_{32}\Omega_c$, $\Omega_2 = a_{42}\Omega_c$, and $\Omega_3 = a_{52}\Omega_c$. Second, such a five-level configuration can be reduced to four-level and three-level configurations by giving $a_{52} = 0$ (in a four-level system) and both $a_{52} = 0$ and $a_{42} = 0$

(in a three-level system). This means that the present model is universal and applicable to various exciting configurations.

## 3. APPLYING TO $^{85}$Rb AND $^{87}$Rb ATOMIC VAPORS

In general, an analytical model can be applied to any atomic or molecular systems that have an energy-level diagram similar to that presented in Fig. 1. In this paper, we apply the analytical model for the Doppler broadened medium for the $5S_{1/2} - 5P_{3/2} - 5D_{5/2}$ transition of $^{85}$Rb atoms [Fig. 2(a)] and $^{87}$Rb atoms [Fig. 2(b)] with selected states as labeled in Fig. 2 [30]. The natural linewidths of the $5P_{3/2}$ and $5D_{5/2}$ states are 6.1 MHz and 0.97 MHz, respectively. For $^{85}$Rb atoms, the probe laser drives the transition $5S_{1/2}$, F = 3 → $5P_{3/2}$, F' = 3, while the coupling laser couples three sets of transitions $5P_{3/2}$, F' = 3 → $5D_{5/2}$, F'' = 4, F'' = 3, and F'' = 2. For $^{87}$Rb atoms, the probe laser drives the transition $5S_{1/2}$, F = 2 → $5P_{3/2}$, F' = 3, and the coupling laser drives three transitions $5P_{3/2}$, F' = 3 → $5D_{5/2}$, F'' = 4, F'' = 3, and F'' = 2. The relative strengths of the three transitions induced by the coupling field are $a_{32} : a_{42} : a_{52} = 1 : 1.46 : 0.6$ for $^{85}$Rb atoms and $a_{32} : a_{42} : a_{52} = 1 : 1.3 : 0.75$ for $^{87}$Rb atoms. The frequency gaps between the hyperfine levels of $^{87}$Rb atoms as $\delta_1 = 28.8$ MHz and $\delta_2 = 22.3$ MHz are greater than those of $^{85}$Rb atoms as $\delta_1 = 9.0$ MHz and $\delta_2 = 7.6$ MHz. This will lead to significant differences in the spectrum of $^{85}$Rb and $^{87}$Rb atoms when the Doppler width is large enough.

First, we study the effect of the Doppler broadening on EIT spectra of $^{85}$Rb and $^{87}$Rb atoms by plotting absorption coefficients with respect to the probe detuning at different temperatures as described in Figs. 3 and 4, respectively. Here, the parameters of the coupling laser are fixed at $\Omega_c = 40$ MHz and $\Delta_c = 0$ (i.e., the coupling laser is resonant with the transition $5P_{3/2}$, F' = 3 → $5D_{5/2}$, F'' = 3), while the temperature is changed as T = 100 K ($W_D = 0.3$ GHz) [Figs. 3(a) and 4(a)], T = 200 K ($W_D = 0.42$ GHz) [Figs. 3(b) and 4(b)], T = 300 K ($W_D = 0.51$ GHz) [Figs. 3(c) and 4(c)], and T = 400 K ($W_D = 0.6$ GHz) [Figs. 3(d) and 4(d)]. It is clear that the absorption spectrum exhibits three transparent windows. For $^{85}$Rb atoms, the positions of the EIT windows are $\Delta_p = -9$ MHz (corresponding to the transition $5P_{3/2}$,
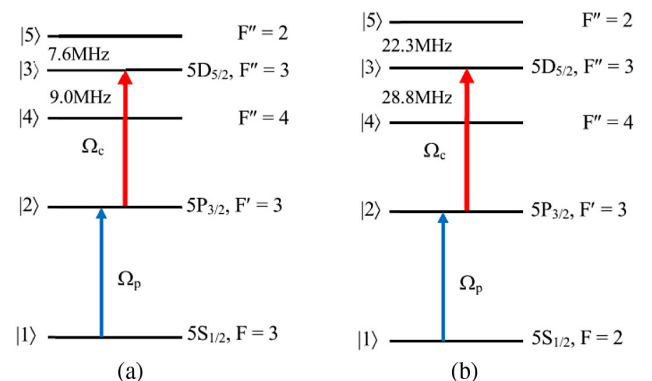


**Fig. 2.** Energy-level diagram of $5S_{1/2} - 5P_{3/2} - 55/2$ transition of (a) $^{85}$Rb atoms and (b) $^{87}$Rb atoms.
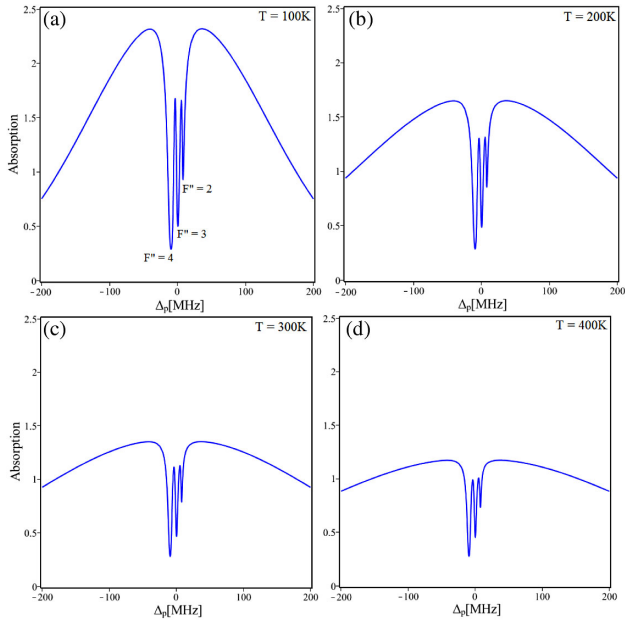
**Fig. 3.** Plots of the absorption coefficient of $^{85}$Rb atoms versus the probe field detuning at different temperatures and (a) T = 100 K, (b) T = 200 K, (c) T = 300 K, and (d) T = 400 K. The parameters of the coupling laser are $\Omega_c = 40$ MHz and $\Delta_c = 0$.
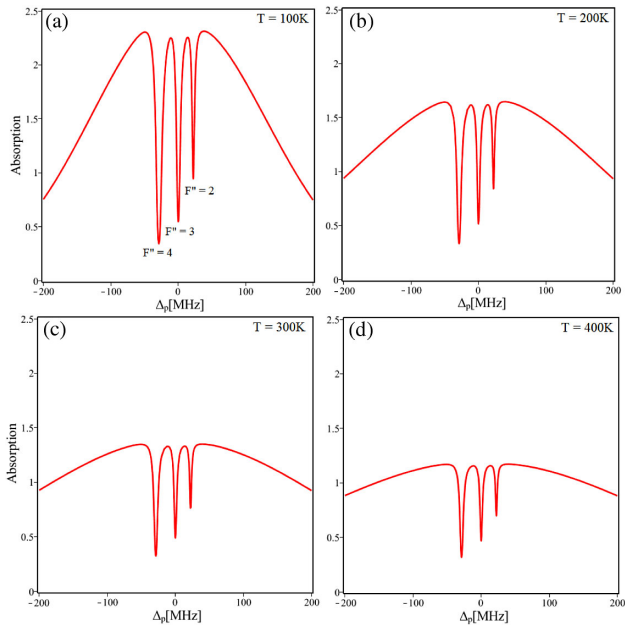


**Fig. 4.** Plots of absorption coefficient of $^{87}$Rb atoms versus the probe field detuning at different temperatures and (a) T = 100 K, (b) T = 200 K, (c) T = 300 K, and (d) T = 400 K. The parameters of the coupling laser are $\Omega_c = 40$ MHz and $\Delta_c = 0$.

F′ = 3 → 5D$_{5/2}$, F″ = 4), $\Delta_p = 0$ (corresponding to the transition 5P$_{3/2}$, F′ = 3 → 5D$_{5/2}$, F″ = 3), and $\Delta_p = 7.6$ MHz (corresponding to the transition 5P$_{3/2}$, F′ = 3 → 5D$_{5/2}$, F″ = 2). For $^{87}$Rb atoms, the positions of the EIT windows are $\Delta_p = -28.8$ MHz (corresponding to the transition 5P$_{3/2}$, F′ = 3 → 5D$_{5/2}$, F″ = 4), $\Delta_p = 0$ (corresponding to the

transition 5P$_{3/2}$, F′ = 3 → 5D$_{5/2}$, F″ = 3), and $\Delta_p = 22.3$ MHz (corresponding to the transition 5P$_{3/2}$, F′ = 3 → 5D$_{5/2}$, F″ = 2). The frequency separations between EIT windows coincide with the frequency gaps between hyperfine levels of the 5D$_{5/2}$ states. When the temperature increases (leading to an increase in Doppler width), therefore, there is overlap between the EIT windows for the $^{85}$Rb atom, while the EIT windows for the $^{87}$Rb atom can still be distinguished, because the frequency gaps between the hyperfine levels of the $^{87}$Rb atom are greater than those of the $^{85}$Rb atom. In general, the EIT windows may not be overlapped when the Doppler shift of the two-photon coherence is smaller than the frequency gap between the transparency peaks [31]. The Doppler shift of the two-photon resonance was calculated as follows [31]:

$$\omega_{two} = (k_p - k_c) \cdot v, \tag{38}$$

where $k_p$ and $k_c$ are the wave vectors of the probe and coupling laser, and $v$ is the velocity of the atom, $v = \sqrt{3k_B T/m}$. Therefore, we derive the condition for temperature as

$$T < \frac{m\delta^2}{12\pi^2 k_B}\left(\frac{\lambda_p \lambda_c}{\lambda_p - \lambda_c}\right)^2, \tag{39}$$

where $\delta$ is the frequency gap between hyperfine levels. Thus, for $^{85}$Rb atoms with $\delta = 7.6$ MHz then T < 500 K, whereas for $^{87}$Rb atoms with $\delta = 22.3$ MHz then T < 3800 K. In addition, to detect such hyperfine components in a weak probe regime, the probe intensity is usually smaller than the saturation intensity of the probe transition, given by $I_{sat} = \frac{\pi}{3}\frac{hc}{\lambda^3 \tau}$, where $\tau = \Gamma^{-1}$ is the lifetime of the upper state and $\lambda$ is the wavelength of the probe laser.

Moreover, we see that the growth of temperature leads depth and width of the EIT windows to decrease significantly. This is because the increase in temperature will reduce the atomic coherence and thus weaken the quantum interference that leads to the EIT effect. We also note that the depth and width of EIT windows are not the same because the relative strengths of the three transitions 5P$_{3/2}$, F′ = 3 → 5D$_{5/2}$, F″ = 4, F″ = 3, and F″ = 2 are different.

Next, we study the influence of the Doppler broadening on the Kerr nonlinearity of the $^{85}$Rb and $^{87}$Rb atoms in the EIT condition by plotting the self-Kerr nonlinear coefficient versus the probe detuning at different temperatures T = 100 K [Figs. 5(a) and 6(a)], T = 200 K [Figs. 5(b) and 6(b)], T = 300 K [Figs. 5(c) and 6(c)], and T = 400 K [Figs. 5(d) and 6(d)]. Other parameters are similar to those in Figs. 3 and 4. From the figures, we see that due to generation of three EIT windows on the absorption line, the Kerr nonlinear coefficient also exhibits a line profile with three normal dispersive curves inside the transparent windows. This means that there are three pairs of negative–positive values of Kerr nonlinear coefficient around positions $\Delta_p = -9$ MHz, $\Delta_p = 0$, and $\Delta_p = 7.6$ MHz for the $^{85}$Rb atom or at positions $\Delta_p = -28.8$ MHz, $\Delta_p = 0$, and $\Delta_p = 22.3$ MHz for the $^{87}$Rb atom. Therefore, the Kerr nonlinear coefficient of the five-level ladder-type system is enhanced simultaneously at different frequencies. Due to the large frequency gaps between the hyperfine levels in the 5D$_{5/2}$ state of the $^{87}$Rb atom, the nonlinear coefficient is enhanced at far more resonant regions than in the case of the $^{85}$Rb atom.
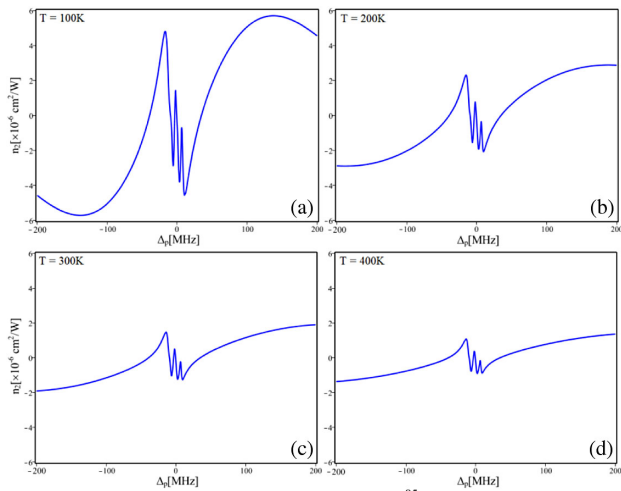
**Fig. 5.** Plots of self-Kerr nonlinear coefficient of $^{85}$Rb atoms versus the probe field detuning at different temperatures and (a) T = 100 K, (b) T = 200 K, (c) T = 300 K, and (d) T = 400 K. The parameters of the coupling laser are $\Omega_c = 40$ MHz and $\Delta_c = 0$.
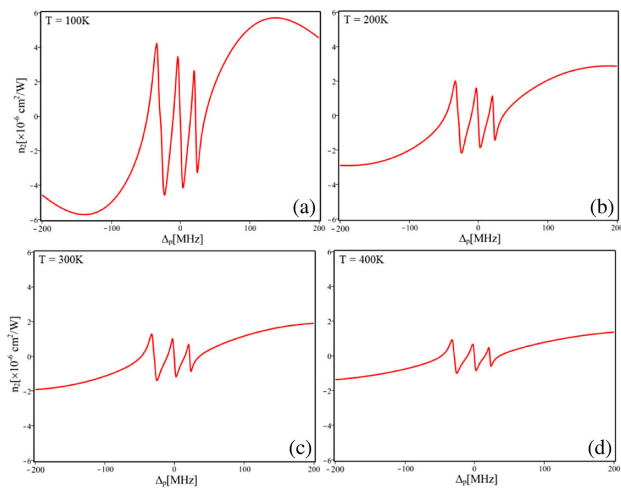


**Fig. 6.** Plots of self-Kerr nonlinear coefficient of $^{87}$Rb atoms versus the probe field detuning at different temperatures and (a) T = 100 K, (b) T = 200 K, (c) T = 300 K, and (d) T = 400 K. The parameters of the coupling laser are $\Omega_c = 40$ MHz and $\Delta_c = 0$.



**Fig. 7.** Plots of self-Kerr nonlinear coefficient of (a) $^{85}$Rb atoms and (b) $^{87}$Rb atoms versus the temperature when $\Omega_c = 40$ MHz, $\Delta_c = 0$, and $\Delta_p = -2$ MHz for $^{85}$Rb atoms and $\Delta_p = 20$ MHz for $^{87}$Rb atoms, which corresponds to one peak of nonlinearity in Figs. 3 and 4, respectively.



**Fig. 8.** Plots of self-Kerr nonlinear coefficient of $^{85}$Rb atoms versus the coupling field detuning at different temperatures and (a) T = 100 K, (b) T = 200 K, (c) T = 300 K, and (d) T = 400 K. Other parameters are $\Omega_c = 40$ MHz and $\Delta_p = 0$.

We also see that, under the influence of Doppler broadening, the profile of the nonlinear coefficient is greatly broadened, and therefore the normal dispersive curves are compressed. Especially when the temperature increases, the amplitude of the normal dispersive curves (appearing in the EIT windows) is significantly reduced. To see this reduction quantitatively, in Fig. 7, we plot the nonlinear coefficient according to the temperature when fixing parameters of laser fields at $\Omega_c = 40$ MHz, $\Delta_c = 0$, $\Delta_p = -2$ MHz for the $^{85}$Rb atom and $\Delta_p = 20$ MHz for the $^{87}$Rb atom, which corresponds to one peak of nonlinearity in Figs. 3 and 4, respectively.

The coupling frequency dependence of the self-Kerr nonlinear coefficient is illustrated in Fig. 8 for the $^{85}$Rb atom and Fig. 9 for the $^{87}$Rb atom. Here, other parameters are employed
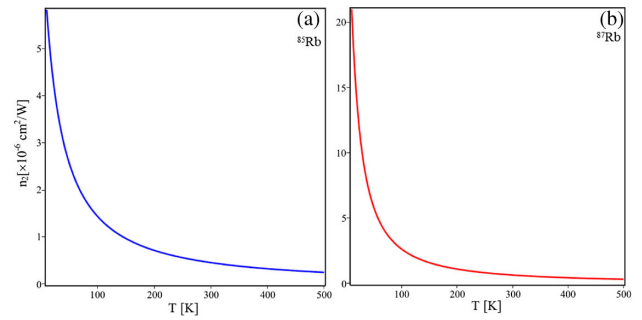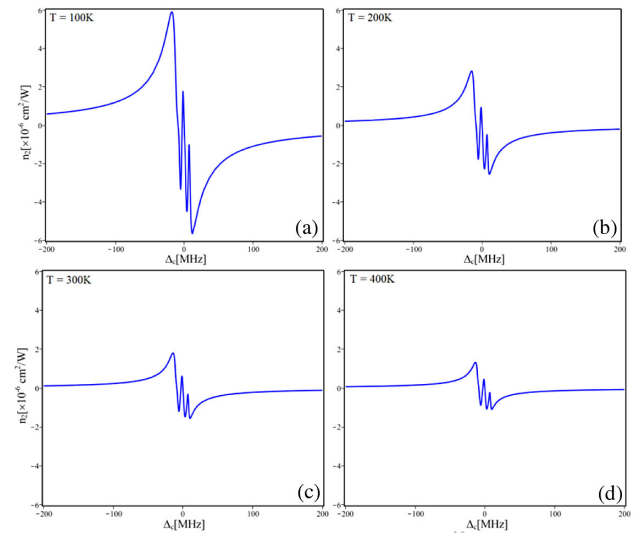
as $\Omega_c = 40$ MHz, $\Delta_p = 0$ (i.e., the probe frequency is resonant with the transition $|1\rangle \rightarrow |2\rangle$), and T = 300 K. This is similar to the probe frequency dependence of the self-Kerr nonlinear coefficient in that there are three normal dispersive curves appearing in the EIT windows. The positions of these dispersive curves are also localized at $\Delta_c = -9$ MHz, $\Delta_c = 0$, and $\Delta_c = 7.6$ MHz for the $^{85}$Rb atom or at $\Delta_c = -28.8$ MHz, $\Delta_c = 0$, and $\Delta_c = 22.3$ MHz for the $^{87}$Rb atom. The occurrence of positive–negative pairs of the nonlinear coefficient shows that we can control the amplitude and sign of the nonlinear coefficient (for a given frequency of the probe laser) by changing the frequency of the coupling laser. The same situation can also be performed by adjusting the intensity (Rabi frequency) of the coupling laser, as shown in Fig. 10. Such a nonlinear coefficient with controllable magnitude and sign allows us to control the characteristics of application devices, such as optical bistability, all-optical switching, and so on.
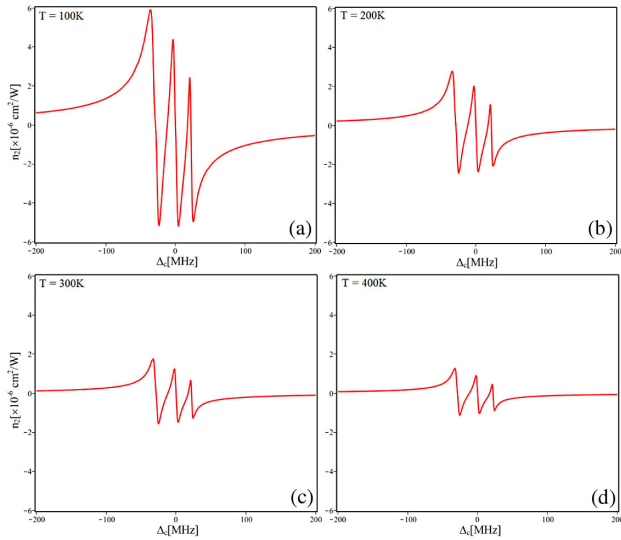
**Fig. 9.** Plots of self-Kerr nonlinear coefficient of $^{87}$Rb atoms versus the coupling field detuning at different temperatures and (a) T = 100 K, (b) T = 200 K, (c) T = 300 K, and (d) T = 400 K. Other parameters are $\Omega_c = 40$ MHz and $\Delta_p = 0$.



**Fig. 11.** Theoretical plots of self-Kerr nonlinear coefficient of $^{87}$Rb atoms versus (a) the probe detuning and (c) the coupling detuning. Experimental measurements of self-Kerr nonlinear coefficient of $^{87}$Rb atoms versus (b) the probe detuning and (b) the coupling detuning [6]. For both cases, the other parameters are $\Omega_c = 72$ MHz and T = 340 K. Solid squares are with EIT and open circles are without EIT.
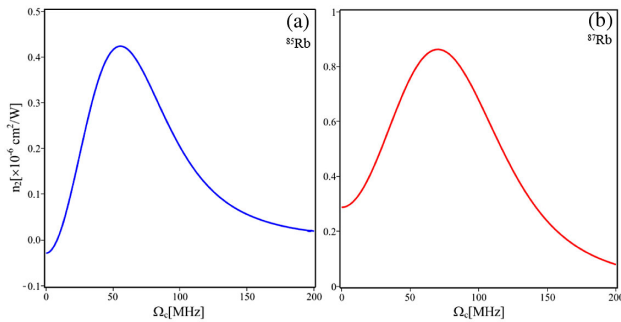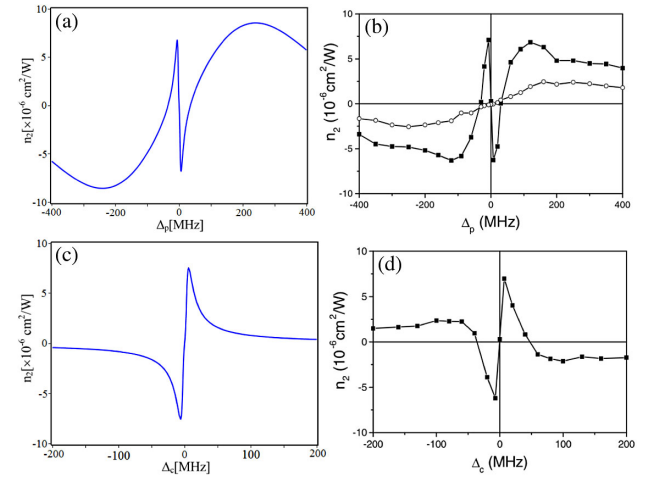


**Fig. 10.** Plots of self-Kerr nonlinear coefficient of (a) $^{85}$Rb atoms and (b) $^{87}$Rb atoms versus the coupling Rabi frequency when T = 300 K, $\Delta_c = 0$, and $\Delta_p = -2$ MHz for $^{85}$Rb atoms and $\Delta_p = 20$ MHz for $^{87}$Rb atoms, which corresponds to one peak of nonlinearity in Figs. 3 and 4, respectively.

Finally, to test the analytical model for self-Kerr nonlinearity under the Doppler effect, we compare the theoretical result with experimental measurement of self-Kerr nonlinearity in Ref. [6] for the case of a hot $^{87}$Rb three-level atomic system (an experimental observation of the self-Kerr nonlinear coefficient in a five-level ladder-type atomic system has not been published so far). In this case, the states $|1\rangle$, $|2\rangle$, and $|3\rangle$ are chosen as $5S_{1/2}$ (F = 1), $5S_{1/2}$ (F = 2), and $5P_{1/2}$ (F' = 2), respectively. In experimental observations for hot atomic vapors, due to a collisional dephasing effect and the laser linewidths, we have to account for their influences in coherence dephasing rates in the density matrix equations by writing decaying rates as $\gamma_{21} \rightarrow \gamma_{21} + \delta\omega_p$ and $\gamma_{31} \rightarrow \gamma_{31} + \delta\omega_c + \gamma_{col}$, where $\gamma_{col}$ presents the collisional dephasing rate, whereas $\delta\omega_p$ and $\delta\omega_c$ are the linewidths of the probe and coupling lasers, respectively [6,15]. By choosing other parameters similar to those in Ref. [6], i.e., $\gamma_{21} = 3.5$ MHz, $\gamma_{31} = 1.1$ MHz, $\Omega_c = 72$ MHz, and T = 340 K, we plot the self-Kerr nonlinear coefficient of $^{87}$Rb

atoms versus the probe detuning and the coupling detuning as displayed in Figs. 11(a) and 11(c), respectively. Experimental measurements of the self-Kerr nonlinear coefficient of the $^{87}$Rb atom versus the probe detuning and the coupling detuning are shown in Figs. 11(b) and 11(d), respectively [6]. The comparisons show that the theoretical curves are in tremendous agreement with the experimental measurements.

## 4. CONCLUSION

We have developed an analytical model to study the influence of Doppler broadening on self-Kerr nonlinearity in a five-level cascade-type atomic system under the EIT condition. The expressions for the first and third susceptibilities and the self-Kerr nonlinearity of a five-level cascade-type atomic medium are found as a function of parameters of the light fields and the temperature of the medium. The analytical model is applied to the transition $5S_{1/2} - 5P_{3/2} - 5D_{5/2}$ of warm $^{85}$Rb and $^{87}$Rb atoms, and it is shown that under the EIT effect, Kerr nonlinearity is enhanced at multiple frequencies with reducing absorption. Besides the enhanced nonlinearity, its amplitude and sign are also controlled according to the intensity and frequency of the coupling laser. When the temperature of atomic vapor increases (i.e., Doppler width increases), the depth and width of the EIT windows decrease accordingly, so the amplitude of the Kerr nonlinear coefficient decreases significantly. In addition, due to the frequency gaps between the superfine levels of the upper excited state of the $^{85}$Rb atom being much smaller than those of the $^{87}$Rb atom, the EIT windows and the nonlinear dispersion curves for the $^{85}$Rb atom are closer than those for the $^{87}$Rb atom. The analytical results agree well with the experimental observation when reducing to a three-level atomic system. The analytical model can be used to fit the experimental observations of self-Kerr nonlinearity in a five-level atomic system under different temperature conditions and

apply to a variety of applications relating to all-optical-switching techniques.

## REFERENCES

1. R. W. Boyd, *Nonlinear Optics* (Academic, 1992).
2. S. E. Harris, "Electromagnetically induced transparency," Phys. Today **50**(7), 36–42 (1997).
3. M. Fleischhauer, A. Imamoglu, and J. P. Marangos, "Electromagnetically induced transparency: optics in coherent media," Rev. Mod. Phys. **77**, 633–673 (2005).
4. H. Schmidt and A. Imamoglu, "Giant Kerr nonlinearities obtained by electromagnetically induced transparency," Opt. Lett. **21**, 1936–1938 (1996).
5. H. Kang and Y. Zhu, "Observation of large Kerr nonlinearity at low light intensities," Phys. Rev. Lett. **91**, 093601 (2003).
6. H. Wang, D. Goorskey, and M. Xiao, "Enhanced Kerr nonlinearity via atomic coherence in a three-level atomic system," Phys. Rev. Lett. **87**, 073601 (2001).
7. K. Nemoto and W. J. Munro, "Nearly deterministic linear optical controlled-NOT gate," Phys. Rev. Lett. **93**, 250502 (2004).
8. A. Joshi and M. Xiao, "Phase gate with a four-level inverted-Y system," Phys. Rev. A **72**, 062319 (2005).
9. Y. Li and M. Xiao, "Enhancement of nondegenerate four-wave mixing based on electromagnetically induced transparency in rubidium atoms," Opt. Lett. **21**, 1064–1066 (1996).
10. V. Tikhonenko, J. Christou, and B. Luther-Davies, "Three dimensional bright spatial soliton collision and fusion in a saturable nonlinear medium," Phys. Rev. Lett. **76**, 2698–2701 (1996).
11. A. Fountoulakis, A. F. Terzis, and E. Paspalakis, "All-optical modulation based on electromagnetically induced transparency," Phys. Lett. A **374**, 3354–3364 (2010).
12. A. Joshi, A. Brown, H. Wang, and M. Xiao, "Controlling optical bistability in a three-level atomic system," Phys. Rev. A **67**, 041801 (2003).
13. D. X. Khoa, L. V. Doai, L. N. M. Anh, L. C. Trung, P. V. Thuan, N. T. Dung, and N. H. Bang, "Optical bistability in a five-level cascade EIT medium: an analytical approach," J. Opt. Soc. Am. B **33**, 735–740 (2016).
14. Y.-Q. Li and M. Xiao, "Electromagnetically induced transparency in a three-level Λ-type system in rubidium atoms," Phys. Rev. A **51**, R2703–R2706 (1995).
15. J. Gea-Banacloche, Y.-Q. Li, S.-Z. Jin, and M. Xiao, "Electromagnetically induced transparency in ladder-type inhomogeneously broadened media: theory and experiment," Phys. Rev. A **51**, 576–584 (1995).
16. Y. Wu and X. Yang, "Electromagnetically induced transparency in V-, Λ-, and cascade-type schemes beyond steady-state analysis," Phys. Rev. A **71**, 053806 (2005).
17. H. Wang, D. Goorskey, and M. Xiao, "Dependence of enhanced Kerr nonlinearity on coupling power in a three-level atomic system," Opt. Lett. **27**, 258–260 (2002).
18. D. McGloin, D. J. Fullton, and M. H. Dunn, "Electromagnetically induced transparency in N-level cascade schemes," Opt. Commun. **190**, 221–229 (2001).
19. E. Paspalakis and P. L. Knight, "Electromagnetically induced transparency and controlled group velocity in a multilevel system," Phys. Rev. A **66**, 015802 (2002).
20. J. Wang, L. B. Kong, X. H. Tu, K. J. Jiang, K. Li, H. W. Xiong, Y. Zhu, and M. S. Zhan, "Electromagnetically induced transparency in multi-level cascade scheme of cold rubidium atoms," Phys. Lett. A **328**, 437–443 (2004).
21. L. V. Doai, P. V. Trong, D. X. Khoa, and N. H. Bang, "Electromagnetically induced transparency in five-level cascade scheme of $^{85}$Rb atoms: an analytical approach," Optik **125**, 3666–3669 (2014).
22. D. X. Khoa, L. C. Trung, P. V. Thuan, L. V. Doai, and N. H. Bang, "Measurement of dispersive profile of a multi-window EIT spectrum in a Doppler-broadened atomic medium," J. Opt. Soc. Am. B **34**, 1255–1263 (2017).
23. J. Sheng, X. Yang, H. Wu, and M. Xiao, "Modified self-Kerr-nonlinearity in a four-level N-type atomic system," Phys. Rev. A **84**, 053820 (2011).
24. H. R. Hamedi and G. Juzeliunas, "Phase-sensitive Kerr nonlinearity for closed-loop quantum systems," Phys. Rev. A **91**, 053823 (2015).
25. H. R. Hamedi, A. H. Gharamaleki, and M. Sahrai, "Colossal Kerr nonlinearity based on electromagnetically induced transparency in a five-level double-ladder atomic system," Appl. Opt. **55**, 5892–5899 (2016).
26. X. D. Yang, S. J. Li, C. H. Zhang, and H. Wang, "Enhanced cross-Kerr nonlinearity via electromagnetically induced transparency in a four-level tripod atomic system," J. Opt. Soc. Am. B **26**, 1423–1434 (2009).
27. J. Kou, R. G. Wan, Z. H. Kang, H. H. Wang, L. Jiang, X. J. Zhang, Y. Jiang, and J. Y. Gao, "EIT-assisted large cross-Kerr nonlinearity in a four-level inverted-Y atomic system," J. Opt. Soc. Am. B **27**, 2035–2039 (2010).
28. D. X. Khoa, L. V. Doai, D. H. Son, and N. H. Bang, "Enhancement of self-Kerr nonlinearity via electromagnetically induced transparency in a five-level cascade system: an analytical approach," J. Opt. Soc. Am. B **31**, 1330–1334 (2014).
29. G. S. He, *Nonlinear Optics and Photonics* (Oxford University, 2015).
30. D. A. Steck, "Rb D line data," http://steck.us/alkalidata.
31. H. Moon and H. Noh, "Comparison between transparencies of $5S_{1/2}$–$5P_{3/2}$–$4D_{5/2}$ and $5S_{1/2}$–$5P_{3/2}$–$5D_{5/2}$ transitions of $^{87}$Rb atoms," J. Opt. Soc. Am. B **29**, 1557–1562 (2012).